Atmospheric, Evolutionary, and Spectral Models of the Brown Dwarf Gliese 229 B

M.S. Marley*, D. Saumon†, T. Guillot†, R.S. Freedman‡, W.B. Hubbard†, A. Burrows§, & J.I. Lunine†

*Department of Astronomy, New Mexico State University, Box 30001/Dept. 4500, Las Cruces NM 88003

†Lunar & Planetary Laboratory, University of Arizona, Tucson AZ 85721

‡Sterling Software, NASA Ames Research Center, Moffett Field CA 94035

§Departments of Physics and Astronomy, University of Arizona, Tucson AZ 85721

Theoretical spectra and evolutionary models that span the giant planet–brown dwarf continuum have been computed based on the recent discovery of the brown dwarf, Gliese 229 B. A flux enhancement in the 4–5 micron window is a universal feature from Jovian planets to brown dwarfs. We confirm the existence of methane and water in Gl 229 B's spectrum and find its mass to be 30 to 55 Jovian masses. Although these calculations focus on Gliese 229 B, they are also meant to guide future searches for extra-solar giant planets and brown dwarfs.

Brown dwarfs inhabit a realm intermediate between the more massive stars and the less massive planets. Their thermal infrared emission is powered by the release of gravitational potential energy as regulated by their atmospheres. Long known only as theoretical constructs, the discovery of the first unimpeachable brown dwarf (1,2) allows a detailed study of a representative of this population of objects. Gliese 229 B, the recently-discovered companion to Gliese (Gl) 229 A, has an estimated luminosity of $6.4 \pm 0.6 \times 10^{-6} L_{\odot}$ (solar luminosity), an effective temperature, $T_{\rm eff}$, below 1200 K, and a clear signature of methane in its spectrum (3). Since there can be no stars cooler than 1700 K, with luminosities below $5 \times 10^{-5} L_{\odot}$, or with methane bands (4), Gl 229 B's status as one of the long-sought brown dwarfs is now beyond question. However, models of Gl 229 B's atmosphere and evolution are required to derive its physical properties and the previous lack of observations had inhibited the generation of theoretical spectra. To remedy this, we coupled model spectra and evolutionary calculations to estimate the object's $T_{\rm eff}$, L, surface gravity g, mass M, radius R, and age t, and to find useful spectral diagnostics. The recent discoveries of planets 51 Pegasi B, 70 Virginis B, 47 Ursae Majoris B, and Gl 411 B (5) have doubled the number of known Jovian planets. There is now an extraordinarily rich variety of low-temperature, low-mass (0.3 – 84 $M_{\rm J}$ (Jupiter mass)) planets and brown dwarfs. Our improved evolutionary models and spectra, here applied to Gl 229 B, are meant to facilitate the study and interpretation of these objects.

To compute the atmospheric temperature profile for brown dwarfs in the relevant temperature range (600–1200 K), we adapt a model originally constructed to study the atmospheres of the Jovian planets and Titan (6). We assume a standard solar composition for the bulk of the atmosphere (7). Refractory elements (for example Fe, Ti, and silicates) condense deep in the atmosphere for $T_{\rm eff} \approx 1000$ K, and thus have negligible gas-phase abundance near the photosphere, as is also true in the atmosphere of Jupiter ($T_{\rm eff} = 124$ K). For an atmosphere similar to that of Gl 229 B, chemical equilibrium calculations indicate that C, N, O, S, and P are found mainly in the form of methane (CH_4), ammonia (NH_3), water (H_2O), hydrogen sulfide (H_2S), and phosphine (PH_3), respectively. However, deep in the atmosphere, chemical equilibrium favors CO over CH_4 and N_2 over NH_3. Our model atmosphere incorporates opacities of these molecules, H_2, and He (8) in their respective solar abundances and includes no other elements.

To constrain the properties of Gl 229 B, we construct a grid of brown dwarf model atmospheres with $T_{\rm eff}$

ranging from 600 to 1200 K and $100 < g < 3200$ m s^{-2}. For each case we compute a self-consistent radiative-convective equilibrium temperature profile and the emergent radiative flux (9). Absorption of radiation from Gl 229 A is included in our model, but contributes negligibly to Gl 229 B's energy balance owing to the large orbital separation (≥ 44 AU) and faintness of Gl 229 A.

Emergent spectra of brown dwarf atmosphere models compared to observed fluxes (Fig. 1) (1,10) show the influence of a minimum in the molecular opacities at wavelengths around $4 - 5$ μm. As in the case for Jupiter, this minimum allows radiation to escape from deep, warm regions of the atmosphere. Clearly, this wavelength region is advantageous for future brown dwarf searches. By comparison, the widely-used K band at 2.2 μm is greatly suppressed by strong CH_4 and H_2-H_2 absorption features. Beyond 13 μm, the decreasing flux falls slightly more rapidly than a Planck distribution with a brightness temperature near 600 K.

Our computed spectra (Fig. 1) are a good match with the data in the $1.2 - 1.8$ μm window regions, but deviate at 1 μm, in the window centered on 2.1 μm, and in regions of low flux. Our best-fitting models reproduce the observed broad band fluxes (3) reasonably well. While many individual spectral features of CH_4 and H_2O are reproduced, particularly near 1.7 and 2.0 μm, the overall band shapes are not well accounted for in the 1 – 2.5 μm region (Fig. 1a). We attribute these discrepancies to a poor knowledge of the CH_4 opacity and, to a lesser extent, the H_2O opacity. Although we have combined several sources of varying accuracy (8) to generate as complete a description of the CH_4 opacity as possible, methane line lists are based on laboratory measurements at room temperature and do not include lines from higher energy levels that would be populated at brown dwarf temperatures. Thus, the opacity of CH_4 at $T \approx 1000$ K is the most likely cause of the mismatches seen in the 1.6 – 1.8 μm band and at $\lambda > 2.1$ μm.

Clouds may alter the atmospheric structure and spectrum of Gl 229 B, as they do in the atmospheres of planets of our solar system. Extrapolating from results for Jupiter (11) and using more recent chemical equilibrium calculations (12), we find that the following additional molecules are expected to condense between 10^{-3} and 10 bars: $NH_4H_2PO_4$, ZnS, K_2S, Na_2S, and MnS. If a relatively large proportion of condensed particles is retained in the atmosphere, cloud layers could affect the structure of the brown dwarf, making it hotter by as much as 100 K at 1 bar (depending on the uncertain particle sizes and optical

properties). Clouds might increase the flux in the K band, due to the higher temperatures, and lower the flux below 1.3 μm, due to scattering.

Given these uncertainties, our best fits for the bolometric luminosity, the observed spectrum, and the photometry give combinations of $T_{\rm eff}$ and g lying in the range $850 < T_{\rm eff}\,({\rm K}) < 1100$ and $g < 3000\,{\rm m\,s^{-2}}$ (Fig. 2). Lower $T_{\rm eff}$ are allowed for $g < 300\,{\rm m\,s^{-2}}$, but the shapes of the J and H bands increasingly deviate from the observations. The high-$T_{\rm eff}$ limit arises from the inability to fit simultaneously the bolometric luminosity and the 10 μm flux.

A determination of Gl 229 B's gravity via spectral matching would impose a direct constraint on its mass. Although g is a function of both mass and radius, the radii of brown dwarfs in this temperature range vary relatively little as the mass varies by an order of magnitude. However, at the present stage of the analysis the gravity is poorly constrained since high g, high $T_{\rm eff}$ models fit the spectra as well as lower g and $T_{\rm eff}$ ones. The model spectra suggest that high spectral resolution ($\lambda/\Delta\lambda \gtrsim 1000$) observations at 1.8–2.1 μm may provide a tighter constraint on g.

The depth at which the atmosphere becomes convective depends upon the specified model gravity and effective temperature. At the highest-pressure point of each model atmosphere, where the temperature-pressure profile merges with an adiabat, the interior entropy is calculated for the purpose of matching an interior temperature distribution to the given values of $(T_{\rm eff}, g)$. The full evolutionary behavior of a brown dwarf is obtained by supplementing previous boundary conditions for objects with masses $\sim 0.3 - 15\,M_J$ (Jupiter mass units) (13, 14) with our grid of nongrey model atmospheres. Such evolutionary models are needed because R varies with mass and age by up to 30%. The precise radius of the object is important because we must match not only Gl 229 B's spectrum, but also the inferred bolometric luminosity: $L = 4\pi R^2 \sigma T_{\rm eff}^4$ (σ is the Stefan-Boltzmann constant). Our results can be summarized by the following approximate fitting formulas (g in m s^{-2}, $T_{\rm eff}$ in K):

$$M = 36\,M_J\,(g/1000)^{0.64}\,(T_{\rm eff}/1000)^{0.23}, \tag{1}$$

$$t = 1.1\,{\rm Gyr}\,(g/1000)^{1.7}\,(T_{\rm eff}/1000)^{-2.8}, \tag{2}$$

$$R = 67200\,{\rm km}\,(g/1000)^{-0.18}\,(T_{\rm eff}/1000)^{0.11}. \tag{3}$$

The effective temperature and surface gravity of Gl 229 B can now be constrained by three sets of observations (which are not independent of each other): (i) the observed spectrum from 1 to 2.5 μm; (ii) the broadband flux in several bandpasses from 2 to 13 μm (10); and (iii) the bolometric luminosity of the object (3). These constraints then limit $g < 2200\,\mathrm{m\,s^{-2}}$ and $T_{\rm eff} = 960 \pm 70\,\mathrm{K}$ (Fig. 2). Since the reported age of Gl 229 A is $\gtrsim 1\,\mathrm{Gyr}$ (1), g is further constrained to lie in the range 800 to $2200\,\mathrm{m\,sec^{-2}}$ (Fig. 3).

In the atmospheres of Gl 229 B and Jupiter, convection commences as the optical depth to thermal photons becomes large, and the temperature profile closely approaches an adiabatic profile at deeper levels owing to efficient convection (Fig. 4). In some models, particularly the lower gravity models and those with $T_{\rm eff} < 900$ K, the radiative-equilibrium lapse rate exceeds the adiabatic lapse rate over a several-bar region near 1 bar. These atmospheres exhibit two convective regions, a lower region, presumably continuing to great depth, and an upper, detached convective zone. Such a detached convective zone is also predicted for the atmosphere of Jupiter (15).

A stellar evolution code and atmosphere models have allowed us to estimate the physical properties of the brown dwarf, Gl 229 B. We derive an effective temperature of 960 ± 70 K and a gravity between 800 and 2200 m s^{-2}. These results translate into masses and ages of 30–55 M_J and 1–5 Gyr, respectively. As Eq 1 and Fig. 3 indicate, gravity maps almost directly into mass, and ambiguity in the former results in uncertainty in the latter. Since the inferred mass of Gl 229 B exceeds that required for deuterium burning (14), deuterium-bearing molecules should not be present in its atmosphere. While the near infrared spectrum of Gl 229 B is dominated by H_2O, we confirm the presence of CH_4 in the atmosphere from our modeling of its features at 1.6–1.8 μm, 2.2–2.4 μm, and 3.2–3.6 μm. In addition, we find a flux enhancement in the window at 4–5 μm throughout the $T_{\rm eff}$ range from 124 K (Jupiter) through 1300 K, and, hence, that this band is a universal diagnostic for brown dwarfs and planets.

References and Notes

1. Nakajima, T. *et al. Nature* **378**, 463 (1995).
2. Oppenheimer, B.R., Kulkarni, S.R., Matthews, K., & Nakajima, T. *Science* **270**, 1478 (1995).
3. Matthews, K., Nakajima, T., Kulkarni, S.R. and Oppenheimer B.R. *Astrophys. J.*, submitted. Geballe, T.R., Kulkarni, S.R., Woodward, C.E., and Sloan, G.C. *Astrophys. J. Lett.*, in press.
4. Burrows, A., Hubbard, W. B., Saumon, D., & Lunine, J. I. *Astrophys. J.* **406**, 158 (1993); Lunine, J.I., Hubbard, W.B. and Marley, M.S. *Astrophys. J.*, **310**, 238 (1986).
5. Mayor, M. & Queloz, D. *Nature*, **378**, 355 (1995); Marcy, G.W., & Butler, R.P. *Astrophys. J. Lett.*, submitted (1996); Butler, R.P. & Marcy, G.W. *Astrophys. J. Lett.*, submitted (1996); Gatewood, G. *BAAS*, in press.
6. McKay, C.P, Pollack, J.B., & Courtin, R. *Icarus* **80**, 23 (1989); Marley, M.S., McKay, C.P., & Pollack, J.B. *Icarus*, submitted.
7. Anders, E., & Grevesse, N. *Geochim. Cosmochim. Acta* **53**, 197 (1989).
8. The opacity calculations include collision-induced absorption by H_2-H_2 [Borysow, A. & Frommhold, L. *Astrophys. J.* **348**, L41 (1990)] and H_2-He [Zheng, C. & Borysow, A. *Icarus* **113**, 84 (1995)] and references therein, free-free absorption by H_2^- [Bell, K.L. *J. Phys. B* **13**, 1859 (1980)], bound-free absorption by H^- [John, T.L. *Astron. & Astrophys.* **193**, 189 (1988)], and Rayleigh scattering. The absorptions of NH_3, CH_4, and PH_3 were calculated using the HITRAN data base [Hilico, J.C., Loete, M., & Brown, L.R., Jr. *J. of Mol. Spectr.* **152**, 229 (1992)] with corrections and extensions. Additional tabulations [Strong, K., Taylor, F.W., Calcutt, S.B., Remedios, J.J., & Ballard, J. *J. Quant. Spectr. Radiat. Transfer* **50**, 363 (1993)] were used where necessary for CH_4, especially shortwards of 1.6 μm. Data for H_2O and H_2S were computed from a direct numerical diagonalization [Wattson, R.B., and Rothman L.S. *JQSRT* **48**, 763 (1992)] by R.B. Wattson (personal communication). Absorption by CO [Pollack *et al. Icarus* **103**, 1 (1993)] and PH_3 opacity was included in the spectral models, but not in the temperature profile computation. The baseline models assume the atmosphere to be free of clouds.
9. For the temperature profile computation, molecular opacity was treated using the k-coefficient method [Goody, R., West, R., Chen, L., & Crisp, D. *J. Quant. Spectr. Radiat. Transfer* **42**, 539 (1989)].

After a radiative-equilibrium temperature profile was found, the atmosphere was iteratively adjusted to self-consistently solve for the size of the convection zones, given the specified internal heat flux. Given the radiative-convective temperature-pressure profiles, high-resolution synthetic spectra were generated by solving the radiative transfer equation [Bergeron, P., Wesemael, F., and Fontaine, G. *Ap.J.* **367**, 253 (1991)] Eighteen thousand frequency points were used in the 1 – 15.4 μm spectral region. These spectra were smoothed with a Gaussian-bandpass filter giving a final resolution of $\lambda/\Delta\lambda = 600$.

10. Matthews, K., Nakajima, T., Kulkarni, S., & Oppenheimer, B. *IAU Circ. #6280* (1995).
11. Fegley, B., Jr & Lodders, K. *Icarus* **110**, 117 (1994).
12. K. Lodders (personal communication).
13. Burrows, A., Saumon, D., Guillot, T., Hubbard, W.B., & Lunine, J.I. *Nature* **375**, 299 (1995).
14. Saumon, D., *et al. Astrophys. J.* **460**, 993 (1996).
15. Guillot, T., Gautier, D., Chabrier, G., & Mosser, B. *Icarus* **112**, 337 (1994).
16. Lindal, G. *Astron.J.* **103**, 967 (1992).
17. D.S. is a Hubble Fellow. T.G. is supported by the European Space Agency. This research was supported by grants from the National Aeronautics & Space Administration, and from the National Science Foundation. We thank T. Geballe for digital versions of the Gl 229 B spectrum, K. Lodders for chemical-equilibrium calculations, and K. Zahnle for an insightful review.

Figure Captions

Fig. 1 A): Synthetic spectra for (bottom to top) $T_{\rm eff}$ = 890, 960, 1030 K and g = 1000 m s^{-2}, together with data (3) (red line). The three curves in B) are calculated for the same values of $T_{\rm eff}$ and g; colored boxes show the photometric measurements with bandpasses indicated by their width. The red region shows the 1σ error on the measurements while yellow gives the 2σ error. Yellow triangles show upper limits to narrow band fluxes. In both panels, spectral intervals are labeled with the molecules primarily responsible for the opacity in that interval.

Fig. 2 Limits on $T_{\rm eff}$ and g of Gl 229 B. The grey shaded area delimits the effective temperature and gravity of model objects which match within 2σ the observed bolometric luminosity (3) of Gl 229 B at any age. The other areas show limits from fitting the $1 - 2.5\,\mu$m spectrum (vertical lines) and the $2.5 - 13\,\mu$m photometry (horizontal lines).

Fig. 3 The grey shaded area shows the region of overlap of the three constraints from Fig. 2 (the cutoff at low g is arbitrary). Solid lines depict the evolution of $T_{\rm eff}$ and g as various mass brown dwarfs cool. Several contours of constant radius (long-dashed curves) and constant age (short-dashed curves) are also shown.

Fig. 4 Calculated atmospheric structure for Gl 229 B; the dashed curve shows an adiabat corresponding to the deep interior temperature profile. For comparison, a profile for Jupiter (16) is shown, along with its calculated prolongation into the adiabatic deep interior (dashed curve).

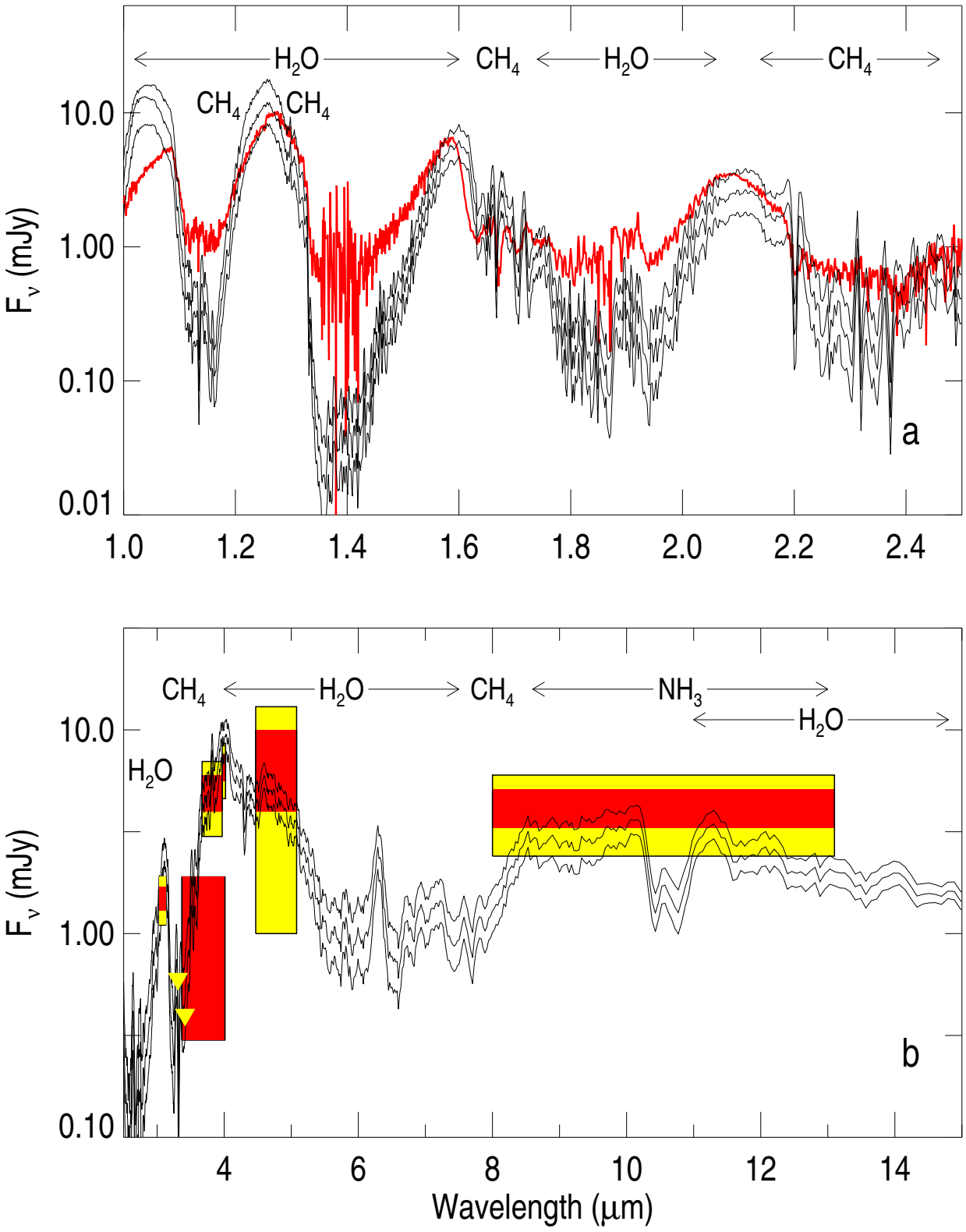
H2O
CH4
H2O
CH4
CH4
CH4
10.0
1.00
0.10
0.01
Fν (mJy)
1.0
1.2
1.4
1.6
1.8
2.0
2.2
2.4
a
CH4
H2O
CH4
NH3
H2O
H2O
10.0
1.00
0.10
Fν (mJy)
4
6
8
10
12
14
Wavelength (μm)
b

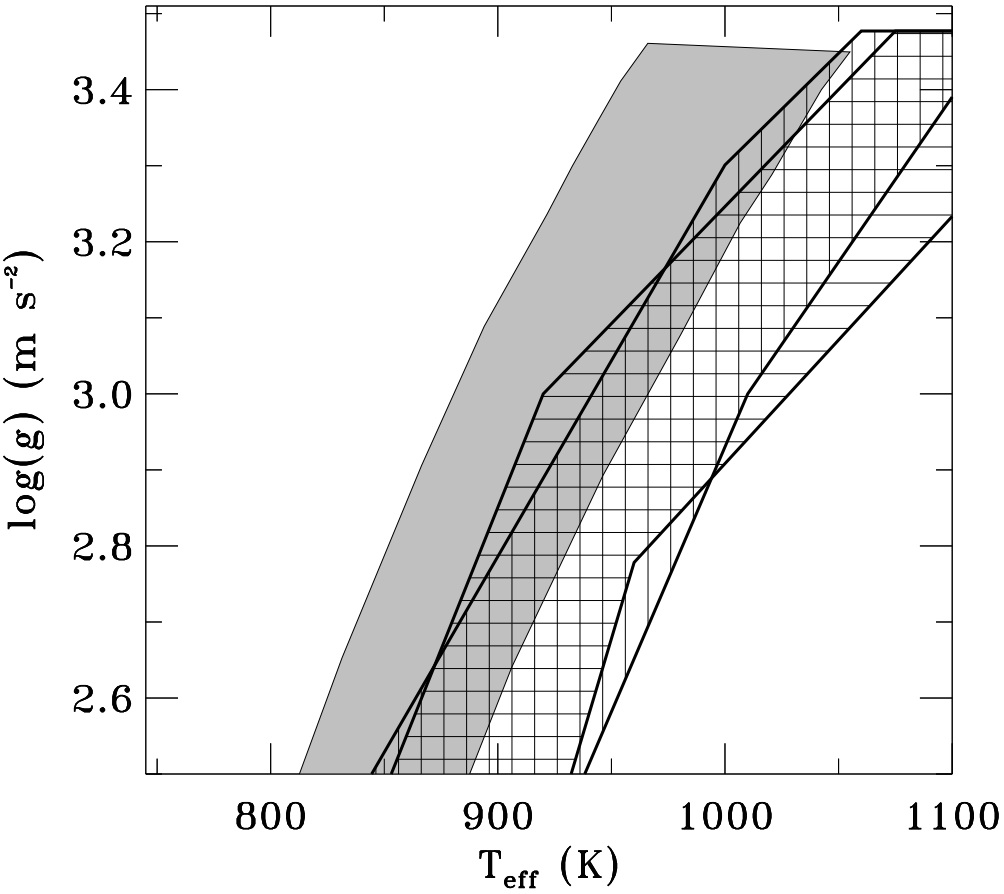
3.4
3.2
3.0
2.8
2.6
log(g) (m s^{-2})
800
900
1000
1100
T_{eff} (K)

Marley et al. Fig. 3 May 30, 1996

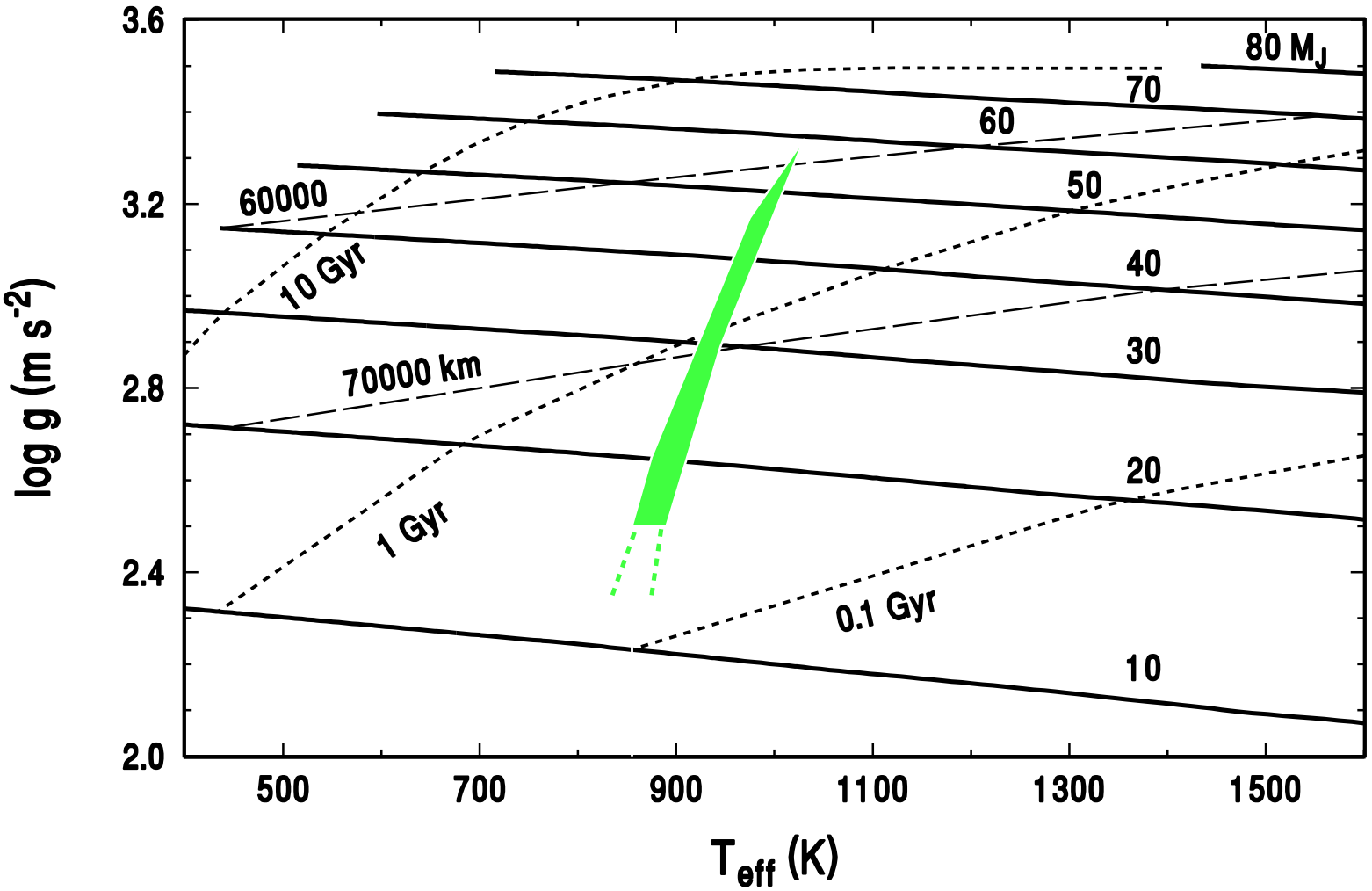

Marley et al., Fig. 4 May 30, 1996